

Supporting Information for:

Visualization of Water-Induced Surface Segregation of Polarons on Rutile TiO₂(110)

Chi M. Yim,^{†,∇} Ji Chen,^{‡,∇} Yu Zhang,[†] Bobbie-Jean Shaw,[†] Chi L. Pang,[†] David C. Grinter,[†] Hendrik Bluhm,^{§,||} Miquel Salmeron,[⊥] Christopher A. Muryn,[#] Angelos Michaelides,[‡] and Geoff Thornton^{*,†}

[†] *Department of Chemistry and London Centre for Nanotechnology, University College London, 20 Gordon Street, London WC1H 0AJ, United Kingdom*

[‡] *Department of Physics and Astronomy, London Centre for Nanotechnology and Thomas Young Centre, University College London, London WC1E 6BT, United Kingdom*

[§] *Chemical Sciences Division, Lawrence Berkeley National Laboratory, Berkeley, California 94720, United States*

^{||} *Advanced Light Source, Lawrence Berkeley National Laboratory, Berkeley, California 94720, United States*

[⊥] *Materials Science Division, Lawrence Berkeley National Laboratory, Berkeley, California 94720, United States*

[#] *School of Chemistry, The University of Manchester, Manchester, M13 9PL, United Kingdom*

*Corresponding author: g.thornton@ucl.ac.uk

TABLE OF CONTENTS

SECTION S1: EXPERIMENTAL DETAILS	3
Scanning Tunneling Microscopy (STM).....	3
Ultraviolet photoelectron spectroscopy (UPS).....	3
Ambient Pressure Photoemission Spectroscopy (APPEs)	4
SECTION S2. COMPUTATION DETAILS	5
SECTION S3. ADDITIONAL DATA ON THE FORMATION OF CONTINUOUS WATER CHAINS	5
Tip-induced Expansion of Perfect Water Film on TiO ₂ (110)	5
Formation of Extended, Nanostructured Water Chains.....	6
SECTION S4: ADDITIONAL DATA FROM DFT CALCULATIONS.....	7
Adsorption Energies of Water Clusters on TiO ₂ (110).....	7
Energy Barrier for Flipping Water Clusters along Ti _{5c} row	7
Repulsive interactions between Water Dimers with Opposite Orientations.....	8
SECTION S5. ADDITIONAL DETAILS ON APPEs MEASUREMENTS	8
Calibration of water coverage.....	8
O 1s core-level spectra	9
Normalization of VB spectra.....	9
SECTION S6. ADDITIONAL STM DATA OF METHANOL ON TiO₂(110).....	10
SUPPORTING FIGURES	11
SUPPORTING REFERENCES	17

Section S1: Experimental Details

Scanning Tunneling Microscopy (STM)

The STM experiments were performed using an *Omicron GmbH* low temperature instrument housed in a bath cryostat in an ultrahigh vacuum (UHV) chamber ($P_{\text{base}} = 2 \times 10^{-11}$ mbar). The adjoining preparation chamber was equipped with sputter ion gun, sample heater, and facilities for low energy electron diffraction (LEED) and X-ray photoelectron spectroscopy (XPS) measurements. Rutile $\text{TiO}_2(110)$ -(1 \times 1) samples were prepared with cycles of argon ion sputtering (1 kV) and vacuum annealing to 1000 K. The sample cleanliness and long-range order were checked using XPS and LEED, respectively. Water dosing was achieved by placing the sample at 78 K in front of a directional doser positioned in the STM chamber. Assuming unity sticking coefficient at 78 K, water exposure that leads to lower water coverage on the $\text{TiO}_2(110)$ surface was calculated from the STM image. Exposure at higher water coverage was determined by extrapolation. Deionized water was used, and was purified by several freeze-pump-thaw (FPT) cycles. STM images were recorded in the constant current mode with electrochemically-etched tungsten tips, conditioned by outgassing at 500 K and voltage pulses in STM. STM measurements were carried out at temperatures between 78 and 170 K. The sample temperature was measured using a silicon diode placed near the sample in the STM stage.

Ultraviolet photoelectron spectroscopy (UPS)

UPS experiments were performed in a separate UHV system ($P_{\text{base}} < 2 \times 10^{-10}$ mbar). A *VG Scienta R3000* hemispherical electron energy analyzer with a He discharge lamp was employed to record the UPS spectra at photon energies of 21.2 and 40.8 eV, respectively. The measurements were carried out with an energy resolution better than 100 meV (full width at half maximum) and at a grazing angle of emission of 15° from the [001] azimuth. The angular resolution of the detector was $\pm 15^\circ$. The position of the Fermi edge was determined from its position in the UPS spectrum of the Ta sample holder.

Ambient Pressure Photoemission Spectroscopy (APPEs)

The APPEs measurements were performed using the end station at the Molecular Environmental Science beamline (11.0.2) of the Advanced Light Source at Lawrence Berkeley National Laboratory. The end station consists of two interconnected UHV chambers, one for APPEs measurements, and another ($P_{\text{base}} = 2 \times 10^{-10}$ Torr) for sample preparation and characterization.¹ The analysis chamber is equipped with a differentially pumped *Specs Phoibos 150* electron spectrometer, allowing for data acquisition at high pressures whilst maintaining the electron analyzer under UHV. Off- and on- resonance valence band (VB) spectra, as well as Ti 3p and O 1s core level spectra were acquired using photon energies of 455, 465.5, 465.5 and 700 eV, respectively. Deconvolution of the spectra was achieved by fitting each individual contribution to a Gaussian-Lorentzian product function, following the subtraction of a Shirley type background to account for the secondary electron emission. The binding energy (BE) scale was aligned with the Ti 3p core levels at 37.5 eV.²

The TiO₂(110)-(1×1) sample was prepared by cycles of argon ion sputtering and annealing in vacuum at 1000 K. Sample temperature was measured using a K-type thermocouple attached to the sample holder. Sample quality was checked using XPS and LEED. This preparation procedure leads to a TiO₂(110) surface populated with surface OH_b, as a result of the reaction of surface O_b-vac with H₂O molecules in the residual vacuum. We denote this surface as *h*-TiO₂.

Mili-Q water was contained within a glass vial attached to the gas line of the UHV system and admitted into the analysis chamber via a high-precision leak valve. Water purification was achieved via FPT cycles. The analysis chamber was flushed with ~0.27 mbar of water before transferring the sample from the preparation chamber in order to displace any contaminants from the chamber walls. To assess damage caused by prolonged photon beam exposure to the sample, we acquired a series of identical spectra from the same area on the sample for an extended period of time. After 20 minutes, the only perceivable change was a small decrease in spectral intensity. To further minimize beam damage, a different area on the sample surface was selected for each new scan/pressure point.

Section S2. Computation Details

Density functional theory (DFT) calculations were performed using the Vienna ab initio simulation package (VASP).^{3,4} Projector augmented-wave (PAW) potentials⁵ were used together with a plane-wave basis set and a cutoff energy of 500 eV for the expansion of the electronic wave functions. The optB86b-vdW^{5,6} exchange correlation functional was used to calculate the adsorption energy of water molecules on the defect free surface. The excess electron states induced by the O_b vacancy was described through the inclusion of an on-site Coulomb interaction with the method introduced by Dudarev⁷ on top of the PBE functional⁸ (PBE+U) and through inclusion of exact exchange using the hybrid HSE functional.⁹ Calculations of the rutile TiO₂ (110) (1×1) surface were performed with periodic slab models of O-Ti-O trilayers. The positions of the bottom two trilayers were fixed during the structure optimizations and a 10 Å vacuum region separated slabs along the surface normal. The main results reported herein were obtained with a (4×2) supercell with 4 trilayers and Brillouin zone sampling with a (2×2×1) Monkhorst-Pack k-point mesh. Minimum energy pathways for the hydrogen bond rearrangement processes of the adsorbed water clusters were calculated using the climbing-image nudged elastic band (CI-NEB) method¹⁰. The structure and charge density images were visualized using the VESTA program.¹¹ The adsorption energy (E_{ad}) is defined as $E_{ad} = (E_{total} - E_{substrate} - N_{molecule} \times E_{molecule}) / N_{molecule}$, where E_{total} is the total energy of the H₂O/TiO₂ system, $E_{substrate}$ the total energy of the TiO₂(110) substrate with no H₂O, $E_{molecule}$ the total energy per H₂O molecule in gas phase, and $N_{molecule}$ the number of H₂O molecules.

Section S3. Additional Data on the Formation of Continuous Water Chains

Tip-induced Expansion of Perfect Water Film on TiO₂(110)

Both the perfect and disordered regions on the water/TiO₂(110) surface (Figure 1d) were stable under normal empty state imaging conditions. However,

when simultaneous empty- and filled- state (or dual-mode) imaging was employed, we observed a lateral expansion of the perfect region (or water film) at the expense of the disordered region. At first (Figure S2a), the perfect region is only present at the bottom right of the frame, whereas in each subsequent image (Figure S2, b and c), it spreads towards the other part of the image so that it almost fills the entire frame (Figure S2c). This suggests that the expansion of the water film was triggered by the rapid switching of the electric field across the tip and sample, induced when the tip changed bias between the forward and backward scans during the dual-mode imaging. Toggling of the electric field direction presumably enables the water clusters to surmount the energy barrier to re-arrange and thereby form continuous chains.

Formation of Extended, Nanostructured Water Chains

Whether the partial water film shown in Figure S2a is formed thermodynamically or by the tip-induced electric field is unclear. In order to shed further light on this, we annealed the sample in Figure S2a to a higher temperature of 170 K and imaged the surface at 78 K. As shown in the empty states image (Figure S3a), the surface is now populated with OH_b (marked with solid circles), a decreased number of H_2O monomers and dimers, and some (~10 nm long) strand features. The filled states image in Figure S3b together with the corresponding line plots in Figure S11c show that the strands are still composed of monomers and dimers. This therefore indicates that the continuous water chains in Figure S2a are not formed thermodynamically and instead result from some STM field-induced process, possibly in combination with the increased temperature.

Owing to their structural difference, nanostructured chains should contain more dangling OH groups compared to continuous chains. Polarized-infrared absorption-reflection spectroscopy could be used to provide additional information regarding the hydrogen bonds forming along water structures.¹²

Section S4: Additional Data from DFT Calculations

Adsorption Energies of Water Clusters on TiO₂(110)

We performed DFT calculations on the stability of different water structures. We first discuss our results on a defect free TiO₂(110) surface. In agreement with previous studies¹³ we find that in the absence of defects, Ti_{5c} sites are the most stable adsorption sites for water molecules and that each molecule forms a hydrogen bond (HB) with an O_b ion (Figure S4a). When additional water molecules attach to the adjacent Ti_{5c} sites, HBs form between water molecules (Figure S4d), leading to the formation of longer chains with a zigzag arrangement (Figure S4g). We calculated the adsorption energy (E_{ad}) for different-sized water clusters using the optB86b-vdW^{5,6} exchange correlation functional. In line with previous calculations,^{14,15} we find that the *continuous* water chains ($E_{ad} = -1.194$ eV/H₂O) are more stable than monomers with the stability increasing slightly with the length of the water chain so that monomers, dimers and trimers have E_{ad} of -1.101, -1.153 and -1.175 eV/H₂O, respectively.

Energy Barrier for Flipping Water Clusters along Ti_{5c} row

The reason *continuous* water chains do not form at 78 K is most likely due to kinetics. To look into this issue we calculated the energy barriers for flipping the orientation of these water structures. Various mechanisms were considered, with the most relevant paths shown in Figure S4. Our calculations show that flipping a monomer has a very low barrier of 53 meV (Figure S4b), so that the formation of dimers is facile. However, flipping a dimer is more difficult: a HB must be broken before it is reformed. As such, the barrier is much higher at 225 meV/molecule (Figure S4e). For a *continuous* water chain, the minimum energy path involves simultaneous rotation of water molecules, and the barrier is similar to that for flipping a dimer at 246 meV/molecule (Figure S4h). Therefore, once a chain of dimer or larger cluster forms, its orientation is unlikely to change. This explains why *continuous* water chains are still not formed on the TiO₂(110) surface even after the surface is annealed to 170 K (Figure S3), even though the average adsorption of water molecules is stronger for longer chains.

Repulsive interactions between Water Dimers with Opposite Orientations

To understand the interactions between water clusters with opposite orientations along the Ti row, we employed DFT to calculate the adsorption energy of two water dimers with different separation distances along the Ti_{5c} row. We considered three different configurations. In the first configuration (Figure S5a), the alignment between dimers is such that they have parallel hydrogen bond (HB) directions that we denote as the *para* configuration, while in the other two configurations the dimers have anti-parallel HB directions with either their O or H atoms facing each other (see Figure S5b,c). We name these two configurations as *anti-O* and *anti-H* configurations, respectively.

Our calculations show that regardless of their configuration, the adsorption energy of two dimers converges to a value of ~ -1.158 to -1.155 eV per molecule after they are separated by three lattice units (i.e. when there are two unoccupied Ti_{5c} sites between them). When two dimers reside in adjacent sites, the *para* configuration has an adsorption energy of -1.180 eV per molecule, while the *anti-O* and *anti-H* configurations have adsorption energies of -1.150 and -1.091 eV per molecule respectively (Figure S5d). This indicates that the interaction between two dimers in the *para* configuration is attractive, while that between the dimers in any of the *anti* configurations is repulsive in nature. As such, the closest possible separation between two dimers in each of the *anti*- configurations is 2-3 lattice units (i.e. when there are 1-2 unoccupied Ti_{5c} sites between them). This means that in order for two dimers to reside at adjacent sites, they must already be oriented with parallel HB.

Section S5. Additional Details on APPEs Measurements

Calibration of water coverage

We calculated the relative humidity (RH) using the sample temperature and water partial pressure (P_{water}) inside the vacuum chamber.¹ The maximum RH to which the sample was exposed is estimated to be $\sim 30\%$. In turn, the knowledge of the RH allows estimation of the water coverage on the surface, expressed in monolayers (ML). On rutile TiO₂(110), 1 ML is defined as one H₂O molecule per primitive

surface unit cell, i.e. a density of $5.2 \times 10^{14} \text{ cm}^{-2}$. In our experiment, the RH onset for water molecular adsorption on the rutile $\text{TiO}_2(110)$ surface is $\sim 1 \times 10^{-5} \%$. A coverage of 1 ML is expected to be achieved at a RH of $\sim 1 \%$, corresponding to $P_{\text{water}} \sim 0.03$ mbar at $T \sim 262$ K. The maximum coverage is registered for the highest RH (27%), and is estimated to be ~ 2.7 ML.

O 1s core-level spectra

Figure S12 shows the O 1s spectra recorded from *h*- TiO_2 and that after H_2O exposure at increasing P_{water} . In addition to the peak at BE = 530.6 eV which corresponds to the lattice O^{2-} ions, the spectrum taken from the *h*- TiO_2 surface also exhibits a peak at BE of ~ 531 eV, indicative of the presence of surface OHs. Introducing H_2O into the chamber to different values of P_{water} leads to the appearance of two other peaks, one of which at ~ 534 eV which we attribute to molecular adsorbed H_2O , another of which at ~ 536 eV to H_2O in the gas phase. Note that during H_2O exposure, we also observed a peak at BE ~ 325.5 eV that starts to show up at $P_{\text{water}} \sim 0.027$ mbar. This indicates the presence of CO_x species, one type of contaminant usually present in high pressure studies.¹⁶ It has been suggested that this peak may arise from the presence of formate. However, flashing our sample to 575 K caused no change to this peak, which would be expected if it indeed derived from this carboxylate^{17,18} or carbonate.¹⁹ We therefore exclude these adsorbates as the source of the contamination observed in our experiment.

Normalization of VB spectra

The VB spectra reported in Figure 3a were normalized to the same intensity at BE ~ 17 eV, at which only inelastic secondary electrons contribute. To further visualize changes in the VB region, the spectra in Figure 3a were then subtracted by that of a clean, adsorbate-free surface (obtained at temperature of 575 K at $P_{\text{water}} = 1 \times 10^{-7}$ mbar), leading to difference spectra shown in Figure 3b. Such a procedure allows for the assessment of the occupied molecular orbital structure of different adsorbates present at the surface, in turn providing insight into the study of adsorbate-substrate interactions.

SECTION S6. Additional STM Data of Methanol on TiO₂(110)

Figure S13 shows the STM images of the *reduced* TiO₂(110) surface, recorded after different exposures to methanol at 78 K. Following an exposure of 0.04 L (Figure S13a), two types of protrusions are formed on the Ti_{5c} rows. One is circular, and the other has an elliptical shape elongated along the Ti_{5c} row. Both types of protrusions have a measured height of 190±20 pm in the empty states STM (see line plots in Figure S13g,h). We assign the circular protrusions to be methanol monomers, and the elliptical features as dimers. A line profile across a dimer (Figure S13h) is asymmetric about the center of the dimer, indicative of its tilted adsorption structure on the TiO₂(110) surface.²⁰

Increasing the methanol exposure leads to the formation of other species. Following an exposure of 0.09 L, short chains are also formed. In STM (Figure S13b,e), each short chain appears to consist of two dimers which are separated from each other by a distance of four lattice unit along [001] (Figure S13i). Also, note that compared to their contrast in the empty states STM images (Figure S13a,b), all the methanol species, including monomers, dimers and short chains, have a better defined appearance in the filled states STM (Figure S13d,e). This is also evident from the line plots from the analogous features in the filled states STM images (Figure S13g-i).

Following a methanol exposure of 0.36 L, continuous chains of methanol molecules are also formed. In STM (Figure S13c,f), they appear to consist of protrusions that are evenly spaced from one another along the [001]. Line profiles taken along one continuous chain (Figure S13j) reveal a separation distance between neighboring protrusions of ~4 Å, larger than one substrate lattice unit (3 Å) along the [001] direction. This suggests that methanol molecules in the continuous chains area are less closely packed than they are in dimer form.

Saturating the surface with methanol followed by flashing to 150 K leads to the formation of an ordered overlayer with a $L(1\times 3)$ unit cell. This $L(1\times 3)$ overlayer of methanol has previously been observed by other techniques,^{20,21} and reported to have a methanol dimer in a tilted adsorption configuration in its unit cell.²⁰

Supporting Figures

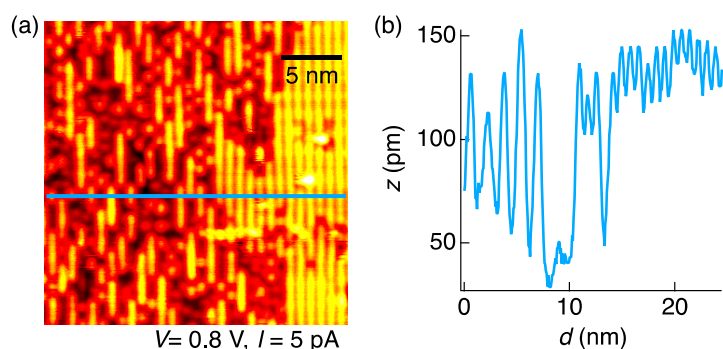


Figure S1. (a) STM image ($T = 146$ K) of $\text{TiO}_2(110)$ recorded after exposure to ~ 0.65 L of H_2O at 78 K, followed by annealing at 146 K. The imaged area consists of both disordered (left) and perfect region (right) (see main text for their definitions). (b) Line plot taken along the line marked in (a).

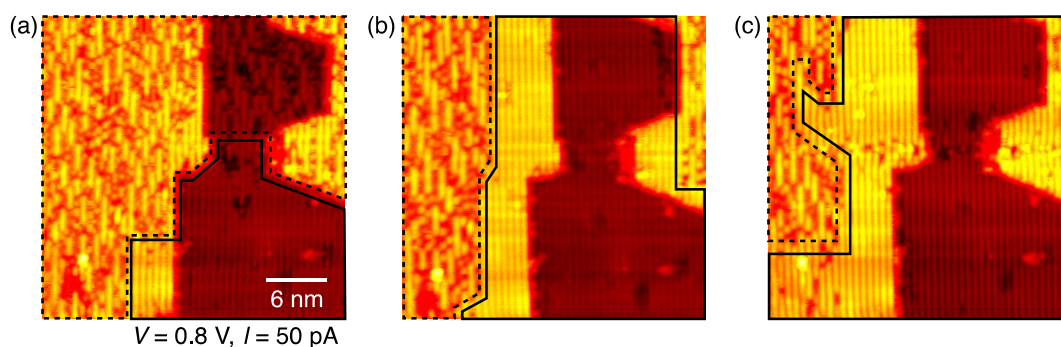


Figure S2. Tip-induced expansion of the perfect water film. (a-c) Empty state STM images recorded sequentially from $\text{TiO}_2(110)$ after exposure to ~ 0.65 L of H_2O at 78 K, followed by annealing at 146 K. Solid (dashed) lines enclose the perfect (disordered) region of the water/ $\text{TiO}_2(110)$ surface (see main text for their definitions). Between the acquisition of each image, toggling of the tip polarity in the attempt to perform dual-mode imaging results in rearrangement of the H_2O molecules on the surface. All images were recorded at 146 K.

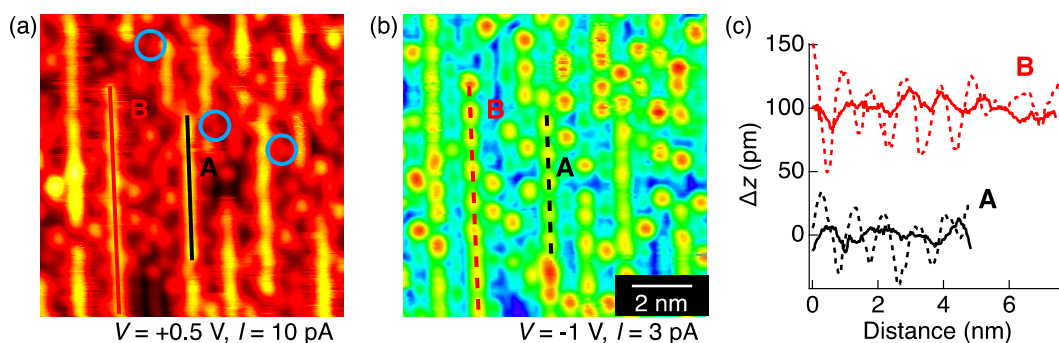


Figure S3. Extended, nanostructured water chains. Dual-mode STM images of *r*-TiO₂(110), recorded after the surface was exposed to ~ 0.65 L of water at 78 K, and then flashed to 170 K, followed by quenching to 78 K. The images were taken at 78 K. In (a), blue circles mark OH_b formed as a result of dissociative H₂O adsorption at O_b-vacs. (c) Line plots along two extended strand features (marked with black and red lines, respectively) measured in both the (a) empty- (solid lines) and (b) filled states images (dashed lines), respectively.

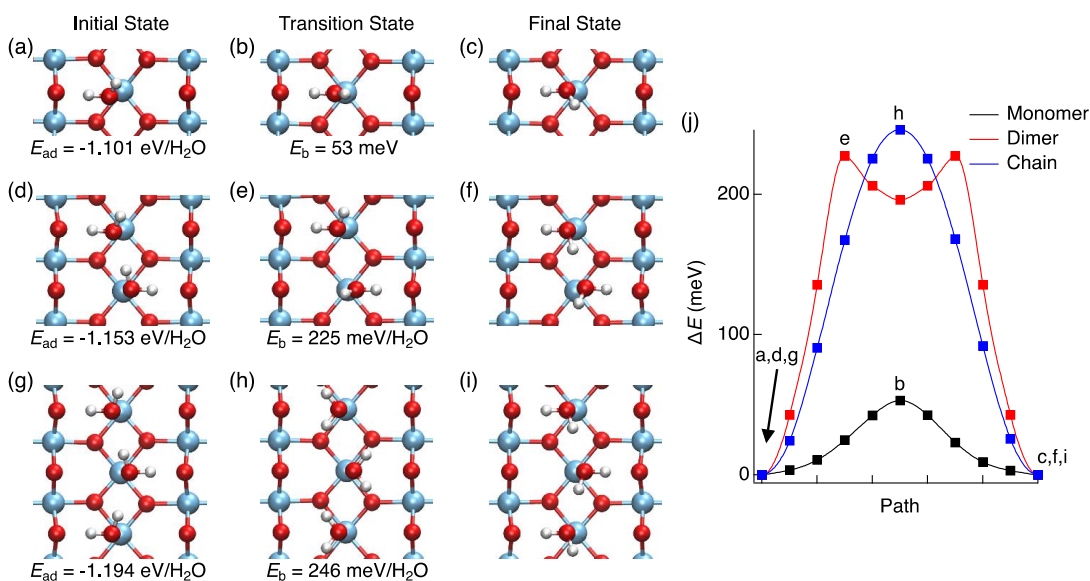


Figure S4. Energy barriers for reorienting small water clusters. The initial, transition, and final state for reorientation of the hydrogen bond direction of (a-c) a water monomer, (d-f) dimer, and (g-i) infinite chain of water molecules on the TiO₂(110) surface. The energy barrier (E_b) for each transition is indicated in (b,e,h) respectively. (j) The energy profiles along the transition paths. The adsorption energy, E_{ad} , for each water species is indicated on the initial states. A (3×2) unit cell is employed for monomer and dimer structures while for the infinite chain structure a (2×2) unit cell is used.

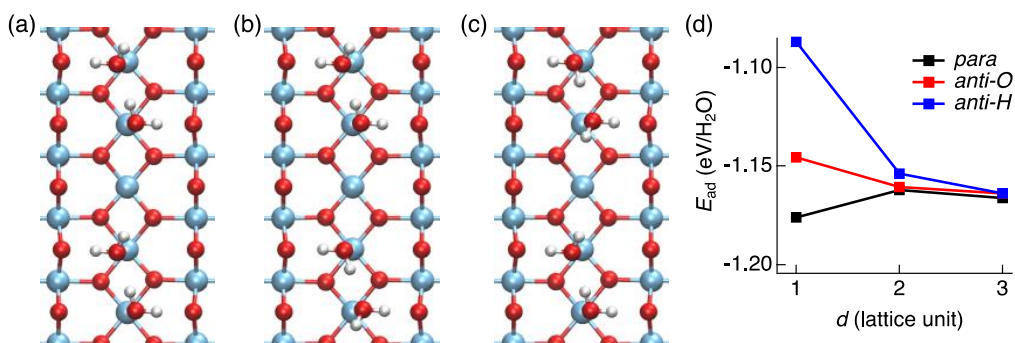


Figure S5. Adsorption energies of two neighboring water dimers. (a-c) Top view of two water dimers residing on the Ti_{5c} row of TiO₂(110), where the dimers are separated from each other by two lattice units (i.e. there is one unoccupied Ti_{5c} site between them). The water dimers are considered to be in three different configurations. In the *para*- configuration in (a), each dimer is oriented with parallel hydrogen bonds (HB) with respect to its neighboring dimer. In the *anti*-configurations in (b-c), they are anti-parallel, with either O atoms (b) or H atoms (c) facing each other. (d) Adsorption energy profiles of two water dimers plotted as a function of their separation distance along the [001], in three different configurations.

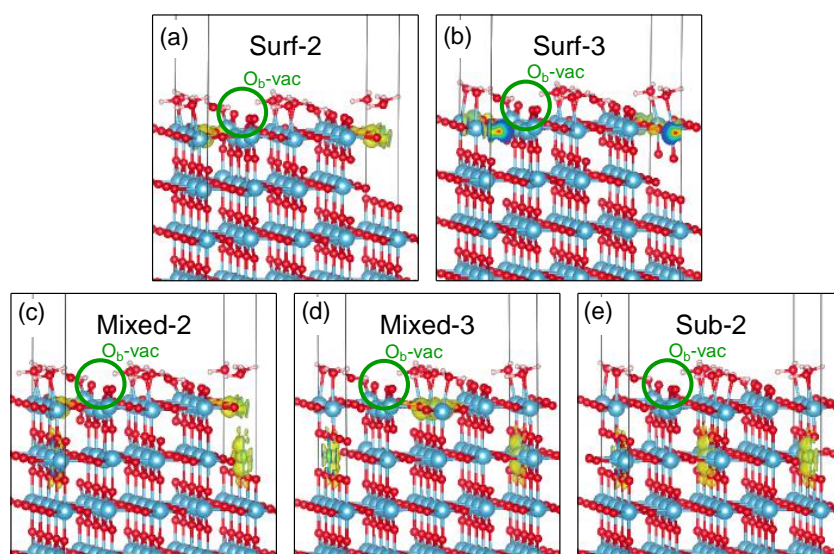


Figure S6. Other configurations of O_b-vac induced excess electrons at different locations on the TiO₂(110) surface covered with 1 ML of H₂O. (a-b) Surf-2 and Surf-3: excess electrons are located in the first layer. (c-d) Mixed-2 and Mixed-3: excess electrons are located in the first and second layer. (e) Sub-2: excess electrons are located in the second layer.

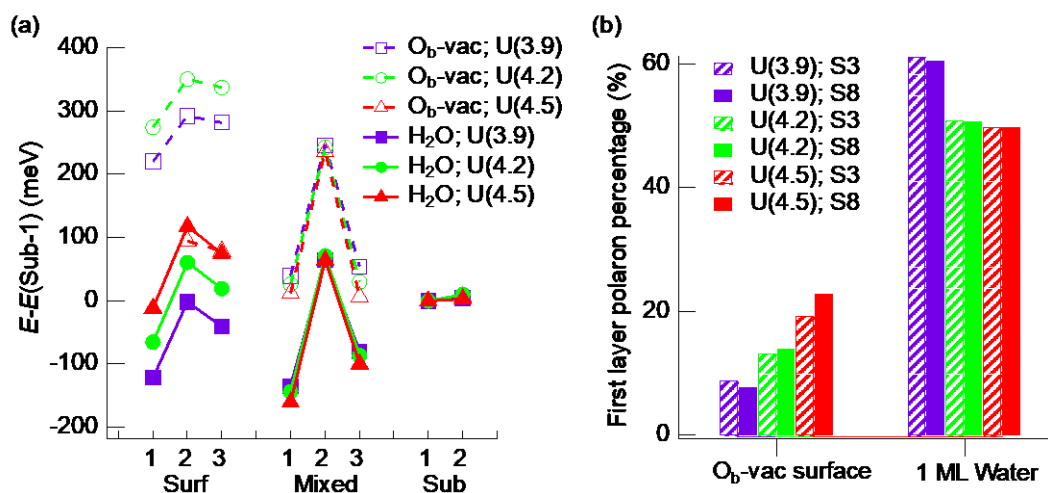


Figure S7. Calculated energies and population of excess electrons in the top surface layer of $r\text{-TiO}_2(110)$ with and without a water film. (a) Relative energies of eight polaron configurations with (H_2O) and without the water film ($O_b\text{-vac}$), calculated using different Hubbard U values. (b) Relative population of excess electrons in the first surface layer of $r\text{-TiO}_2(110)$ without ($O_b\text{-vac}$) and with 1 ML of water at 300 K calculated using different Hubbard U values and comparing an average of 3 (S3) and 8 (S8) configurations.

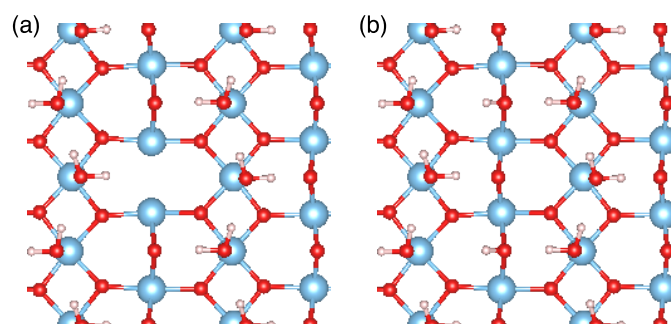


Figure S8. (a) Oxygen vacancy and (b) hydroxylated surface models used for the calculations shown in Figure 2.

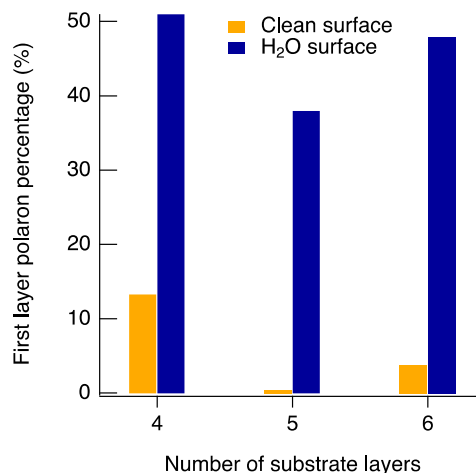


Figure S9. Calculated population of excess electrons on the top layer at 300 K for clean and water covered surfaces. The population is calculated as a function of the number of substrate layers. The estimates are based on a Boltzmann distribution as noted in the main text.

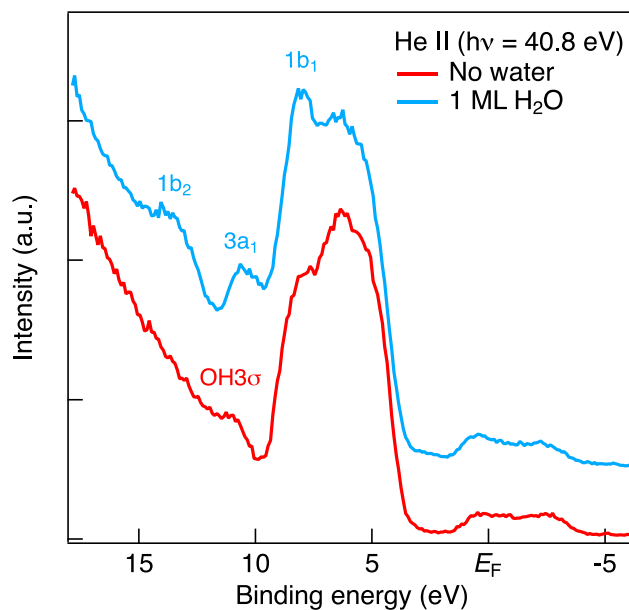


Figure S10. He II ($h\nu = 40.8$ eV) UPS valence band spectra taken before (red) and after (blue) the as-prepared TiO₂(110) surface was dosed with 1 ML of H₂O at ~200 K. The spectra were recorded at a grazing emission angle of 15° from the [001] azimuth at temperature of 200 K. The peaks corresponding to the 1b₂, 3a₁, 1b₁ molecular orbitals of the adsorbed water molecules, as well as the 3σ orbital of the OH_b are indicated.

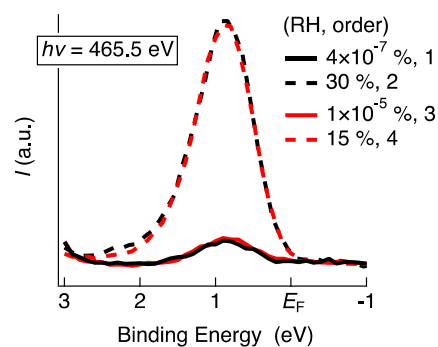


Figure S11. APPEPES spectra of the BGS region of *r*-TiO₂(110) acquired at different relative humidity (RH). In the labels, numbers after the RH values indicate the sequence in which the spectra were taken. The solid black spectrum was recorded from *h*-TiO₂. Spectra are normalized to the O 2s core-level peak at BE ~22.5 eV.

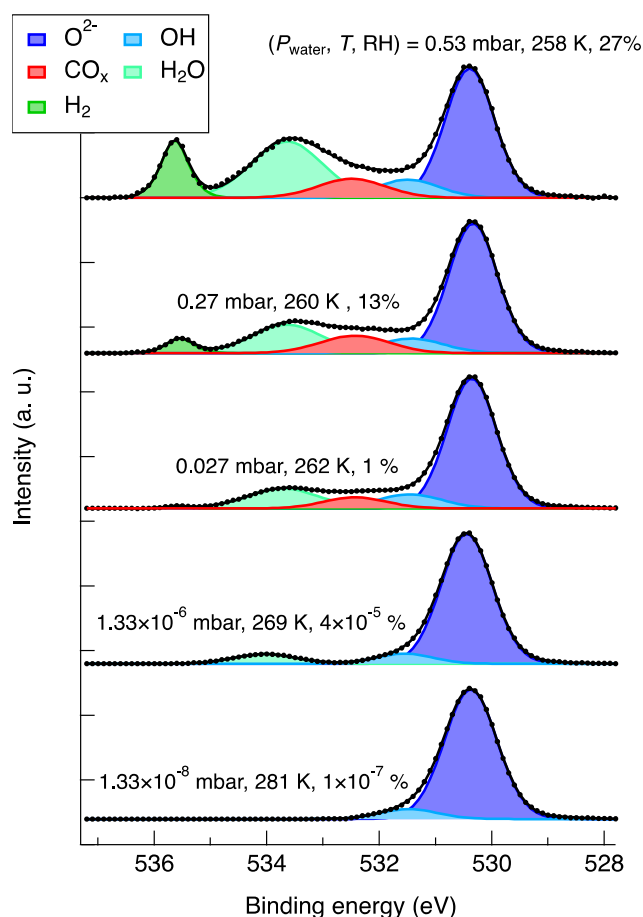


Figure S12. Photoemission spectra of the O 1s region ($h\nu = 700$ eV, $E_{\text{pass}} = 10$ eV) of TiO₂(110) acquired at different water partial pressures (P_{water}). The sample temperatures, and RHs at which the spectra were taken were also indicated. Spectra are normalized to the bulk O²⁻ contribution and are offset vertically for clarity.

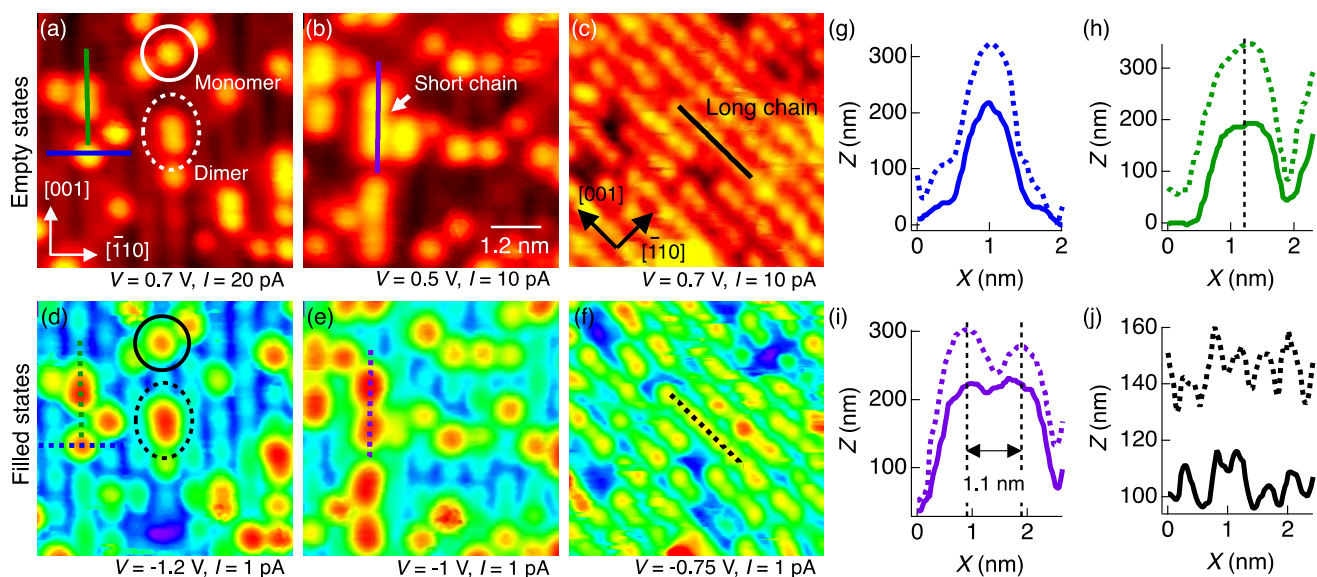


Figure S13. Adsorption configurations of methanol on $\text{TiO}_2(110)$. (a-c) $6 \times 6 \text{ nm}^2$ empty-state STM images recorded from the $r\text{-TiO}_2(110)$ after the surface was exposed to (a) 0.04, (b) 0.09 and (c) 0.36 L of methanol at 78 K. (d-f) Corresponding filled states images to those in (a-c). In (a,d), solid circles mark methanol monomers, dashed circles mark dimers. STM images were recorded at 78 K. (g-j) Line plots taken across monomers (g), dimers (h), short- (i) and continuous chains of methanol molecules (j), marked in the empty- and filled state images in (a-f) respectively.

Supporting References

- (1) Ogletree, D. F.; Bluhm, H.; Lebedev, G.; Fadley, C. S.; Hussain, Z.; Salmeron, M. A Differentially Pumped Electrostatic Lens System for Photoemission Studies in the Millibar Range. *Rev. Sci. Instrum.* **2002**, *73*, 3872–3877.
- (2) Hardman, P. J.; Prakash, N. S.; Muryn, C. A.; Raikar, G. N.; Thomas, A. G.; Prime, A. F.; Thornton, G.; Blake, R. J. Oxygen-Vacancy Sites on $\text{TiO}_2(100)1 \times 3$ Using Surface Core-Level-Shift Photoelectron Diffraction. *Phys. Rev. B* **1993**, *47*, 16056–16059.
- (3) Kresse, G.; Furthmüller, J. Efficient Iterative Schemes for *Ab Initio* Total-Energy Calculations Using a Plane-Wave Basis Set. *Phys. Rev. B* **1996**, *54*, 11169–11186.
- (4) Kresse, G.; Joubert, D. From Ultrasoft Pseudopotentials to the Projector Augmented-Wave Method. *Phys. Rev. B* **1999**, *59*, 1758.
- (5) Klimeš, J.; Bowler, D. R.; Michaelides, A. Chemical Accuracy for the Van Der Waals Density Functional. *J. Phys.: Condens. Matter* **2009**, *22*, 022201.
- (6) Klimeš, J.; Bowler, D. R.; Michaelides, A. Van Der Waals Density Functionals Applied to Solids. *Phys. Rev. B* **2011**, *83*, 195131.
- (7) Dudarev, S. L.; Botton, G. A.; Savrasov, S. Y.; Humphreys, C. J.; Sutton, A. P. Electron-Energy-Loss Spectra and the Structural Stability of Nickel Oxide: an LSDA+U Study. *Phys. Rev. B* **1998**, *57*, 1505–1509.

- (8) Perdew, J. P.; Burke, K.; Ernzerhof, M. Generalized Gradient Approximation Made Simple. *Phys. Rev. Lett.* **1996**, *77* (18), 3865–3868.
- (9) Heyd, J.; Scuseria, G. E.; Ernzerhof, M. Erratum: “Hybrid Functionals Based on a Screened Coulomb Potential” [*J. Chem. Phys.* *118*, 8207 (2003)]. *J. Chem. Phys.* **2006**, *124*, 219906.
- (10) Henkelman, G.; Uberuaga, B. P.; Jónsson, H. A Climbing Image Nudged Elastic Band Method for Finding Saddle Points and Minimum Energy Paths. *J. Chem. Phys.* **2000**, *113*, 9901.
- (11) Momma, K.; Izumi, F. VESTA 3 for Three-Dimensional Visualization of Crystal, Volumetric and Morphology Data. *J. Appl. Crystallogr.* **2011**, *44*, 1272–1276.
- (12) Wang, Y.; Wöll, C. IR Spectroscopic Investigations of Chemical and Photochemical Reactions on Metal Oxides: Bridging the Materials Gap. *Chem. Soc. Rev.* **2017**, *46*, 1875–1932.
- (13) Björneholm, O.; Hansen, M. H.; Hodgson, A.; Liu, L.-M.; Limmer, D. T.; Michaelides, A.; Pedevilla, P.; Rossmeisl, J.; Shen, H.; Tocci, G.; et al. Water at Interfaces. *Chem. Rev.* **2016**, *116*, 7698–7726.
- (14) Kimmel, G. A.; Baer, M.; Petrik, N. G.; VandeVondele, J.; Rousseau, R.; Mundy, C. J. Polarization- and Azimuth-Resolved Infrared Spectroscopy of Water on TiO₂(110): Anisotropy and the Hydrogen-Bonding Network. *J. Phys. Chem. Lett.* **2012**, *3*, 778–784.
- (15) Lee, J.; Sorescu, D. C.; Deng, X.; Jordan, K. D. Water Chain Formation on TiO₂(110). *J. Phys. Chem. Lett.* **2013**, *4*, 53–57.
- (16) Ketteler, G.; Ogletree, D. F.; Bluhm, H.; Liu, H.; Hebenstreit, E. L. D.; Salmeron, M. In Situ Spectroscopic Study of the Oxidation and Reduction of Pd(111). *J. Am. Chem. Soc.* **2005**, *127*, 18269–18273.
- (17) Chambers, S. A.; Thevuthasan, S.; Kim, Y. J.; Herman, G. S.; Wang, Z.; Tober, E.; Ynzunza, R.; Morais, J.; Peden, C. H. F.; Ferris, K.; et al. Chemisorption Geometry of Formate on TiO₂(110) by Photoelectron Diffraction. *Chem. Phys. Lett.* **1997**, *267*, 51–57.
- (18) Henderson, M. A. Complexity in the Decomposition of Formic Acid on the TiO₂(110) Surface. *J. Phys. Chem. B* **1997**, *101*, 221–229.
- (19) Song, A.; Skibinski, E. S.; DeBenedetti, W. J. I.; Ortoll-Bloch, A. G.; Hines, M. A. Nanoscale Solvation Leads to Spontaneous Formation of a Bicarbonate Monolayer on Rutile (110) Under Ambient Conditions: Implications for CO₂ Photoreduction. *J. Phys. Chem. C* **2016**, *120*, 9326–9333.
- (20) Silber, D.; Kowalski, P. M.; Traeger, F.; Buchholz, M.; Bebensee, F.; Meyer, B.; Wöll, C. Adsorbate-Induced Lifting of Substrate Relaxation Is a General Mechanism Governing Titania Surface Chemistry. *Nat. Commun.* **2016**, *7*, 12888.
- (21) Henderson, M. A.; Otero-Tapia, S.; Castro, M. E. The Chemistry of Methanol on the TiO₂(110) Surface: the Influence of Vacancies and Coadsorbed Species. *Faraday Discuss.* **1999**, *114*, 313–329.